Adaptive Critic Design based Dynamic Optimal Power Flow Controller for a Smart Grid

Jiaqi Liang, Ronald G. Harley
School of Electrical and Computer Engineering
Georgia Institute of Technology
Atlanta, GA, USA
jliang@gatech.edu; rharley@ece.gatech.edu

Ganesh K. Venayagamoorthy
Real-Time Power and Intelligent Systems Laboratory
Missouri University of Science and Technology
Rolla, MO 65409, USA
gkumar@ieee.org

***Abstract*—An adaptive critic design (ACD) based dynamic optimal power flow control (DOPFC) is proposed in this paper as a solution to the smart grid operation in a high short-term uncertainty and variability environment. With the increasing penetration of intermittent renewable generation, power system stability and security need to be ensured dynamically as the system operating condition continuously changes. The proposed DOPFC dynamically tracks the power system optimal operating point by continuously adjusting the steady-state set points from the traditional OPF algorithms. The ACD technique, specifically the dual heuristic dynamic programming (DHP), is used to provide nonlinear optimal control, where the control objective is formulated explicitly to incorporate system operation economy, stability and security considerations. A 12 bus test power system is used to demonstrate the development and effectiveness of the proposed ACD-based DOPFC using recurrent neural networks.**

***Keywords*-Adaptive critic designs, dynamic optimal power flow control, power system wide-area control, smart grid, recurrent neural networks, neurocontrol.**

I. INTRODUCTION

With the increasing penetration of intermittent renewable generation, power systems encounter more and more uncertainties and short-term variability. How to operate the power systems in such an environment is still an unanswered challenging question [1], [2]. With the state-of-the-art wind forecasting methods, the hour-ahead forecast errors for a single wind plant are around 10-15% with respect to its actual outputs [3]. With much lower forecast errors for loads, the traditional power system operations are based on existing energy management systems (EMS) with deterministic security-constrained commitment and dispatch processes, which tend to be conservative when intermittent renewable generation is considered [2]. These conservative operations somewhat contribute to a large amount of wind curtailment nowadays [4].

The core EMS application, optimal power flow (OPF) [5], [6] or its security-constrained version, is based on steady-state optimization without considering local controller and load dynamics. Any load/generation variations or post-contingency operations between two dispatch instants (typically 5 minutes) are handled by simple linear regulators, such as automatic generation control (AGC) [7], or some predefined reactions with little, if any, system-wide optimization.

The development of wide-area measurement systems (WAMS), based on synchronized phasor measurement units [8], greatly improves the power grid observability. WAMS enables dynamic state estimation, dynamic generator status monitoring, synchronized substation voltage and current monitoring, and various wide-area control (WAC) schemes that require remote signals [9], [10]. Most of the WAC applications to date have focused on transient/small-signal stabilizing control to mitigate angle instability [11]-[14], secondary voltage control to mitigate voltage instability [15]-[16], and emergency control in response to severe contingencies [17]. The design of a system-wide automatic power flow controller to dynamically control a power system to its optimal operating point has received little attention.

Fardanesh [18] described an ideal control scenario for power systems, where optimal operating conditions were achieved instantaneously by some closed-loop control algorithms, but how to design such a control algorithm remained unanswered. A conceptual framework of dynamic stochastic optimization in power systems using adaptive critic designs (ACDs) [19], [20] was first proposed by Venayagamoorthy [21], and then shown on a small system in [22]. Momoh [23] presented a similar approach for solving the traditional OPF incorporating prediction and optimization over power system stochastic disturbances. However, detailed designs and analyses have not been reported.

A WAMS based dynamic optimal power flow control (DOPFC) scheme for smart grids is proposed in this paper to optimally and dynamically control power flows in a high uncertainty and variability environment. The power system is a multi-input multi-output, nonstationary, nonlinear complex dynamic plant. An ACD-based recurrent neurocontroller is designed to dynamically track the power system optimal operating point by adjusting the steady-state commands set by the traditional OPF algorithm. The ACD technique enables controllers to deal with nonlinear nonstationary systems in the presence of noise and uncertainty [23]. An explicit optimization objective is defined in the ACD technique. Thus, operating cost and different stability and security indices of interest can be easily formulated in the control objective.

This work was supported in part by the National Science Foundation, USA, under Grants ECCS #0348221, ECCS 0802047 and EFRI 0836017.

An overview of the existing system-wide active and reactive power control schemes is provided in Section II with an introduction to the DOPFC concept. Section III provides the mathematical background of using ACD with recurrent neural networks to implement DOPFC. A 12 bus test power system is used as an example in Section IV to design a DOPFC controller using dual heuristic dynamic programming (DHP, a technique in the ACD family). Control results and case studies are provided in Section V to demonstrate the effectiveness of the designed DHP-based DOPFC scheme.

II. Dynamic Optimal Power Flow Control

A. Existing System-Wide Power Flow Control

Traditionally, power systems have separate control loops for active and reactive power control. For short-term active power balancing, power systems rely on AGC with load frequency control (LFC) to regulate the frequency and maintain the real-time generation-demand balance [7]. AGC uses a simple integrator to regulate the area control error, and generation adjustment commands for individual generators are coordinated by predefined ratios or ratios from economic dispatch [7]. In North America, AGC commands are typically updated every 2-4 s. Although AGC/LFC provides system-wide real power control, it treats the grid as a single bus, has no coordination with the system reactive power control, and does not consider the system stability and security.

Reactive power supports are typically provided by locally controlled switched capacitor banks or on-load tap changing (OLTC) transformers. Automatic secondary/regional voltage control is under development in some countries, such as Italy, where its power system is divided into separate voltage regulation regions with each region having its own pilot node (bus) [15], [16]. The main generators in each region are used to regulate the pilot node voltage with a proportional-integral (PI) regulator [15], where commands are updated no longer than every 2 s [16].

These separate secondary active and reactive power control schemes work well when only small variations/disturbances are present in the system. Lack of coordination and optimization, the existing PI-based secondary frequency and voltage control loops may not be able to optimally and securely control the power system in a high short-term variability environment.

B. The DOPFC Scheme

The observability of the power system is assumed to be sufficiently good with WAMS, and continuous snapshots of the power system are assumed available. With a snapshot as input, the DOPFC optimally adjusts the steady-state dispatch commands from OPF, as shown in Fig. 1. To obtain an optimal dynamic dispatch, both the real and reactive power flows are controlled simultaneously. Under a high short-term variability environment, only those continuously adjustable resources are controlled by the DOPFC to continuously track the optimal operating point, leaving the lifetimes of switched capacitor banks and OLTC transformers unaffected.

A nonlinear optimal control strategy is necessary to achieve the DOPFC, where an objective (cost-to-go function) is

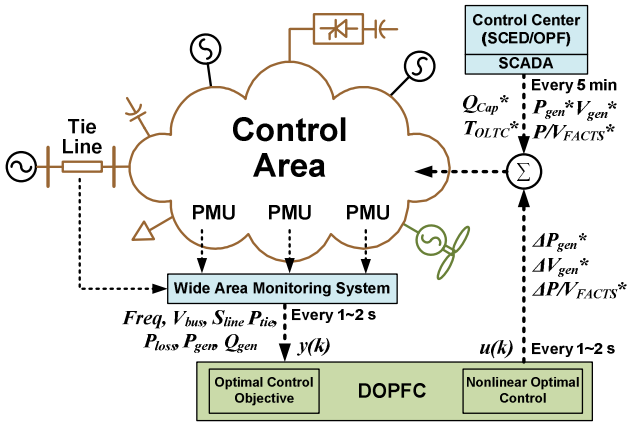

Fig. 1. General framework of DOPFC.

minimized in a closed-loop control fashion and the nonlinearity is used to handle different operating points and physical control limits. Besides the optimality and nonlinearity considerations, the DOPFC must be able to adapt to the time varying dynamics of a power system, whose topology may change at any point in time. To implement DOPFC, it is essential to have a nonlinear optimal control strategy that is able to continuously identify the system topology changes and accordingly adjust its optimal control laws. The ACD technique is a promising candidate and it is used to design the DOPFC controller.

III. Adative Critic Designs with Recurrent Neural Networks for DOPFC

A. Adaptive Critic Desings

A family of ACDs was proposed by Werbos as a new optimal control technique combining the concepts of reinforcement learning and approximate dynamic programming [20]. The ACD technique uses a neural network, namely the critic network, to approximate the cost-to-go function in the Bellman's equation of dynamic programming, as in

$$J(k) = \sum_{i=0}^{\infty} \gamma^i \cdot U(k+i), \tag{1}$$

where γ ($0 < \gamma < 1$) is a discount factor, and $U(k)$ is the utility function (a current cost to be minimized at time k). The optimal control problem is to generate the control action, $u(k)$, that minimizes $J(k)$ at each time step k. For DOPFC, $U(k)$ could be a function of the total energy cost, bus voltage deviations, frequency deviation, tie line flow deviation, line loading, line losses, generator stability margins, and/or other indices related to the system economy, stability and security.

A nonlinear dynamic plant can be described as

$$\begin{aligned} x(k+1) &= F[x(k), u(k)] \\ y(k+1) &= H[x(k+1)] = HF[x(k), u(k)] \end{aligned} \tag{2}$$

where $x(k)$ is the plant state vector and $y(k)$ is the plant output vector. When the nonlinear plant states, $x(k)$, are accessible (available as feedback) and the control law is a function (static or dynamic) of the plant states, i.e., $u(k) = C[x(k)]$, it has been shown that the cost-to-go function, $J(k)$, depends only on the current plant states [23], i.e., $J(k) = V[x(k)]$. The critic network

then approximates this V function with the plant states as its inputs. A second neural network, namely the action network, is used to approximate the optimal control laws, $C_{\text{opt}}[\cdot]$, also with the plant states as its input. A third neural network, namely the model network, is used to model the plant, $F[\cdot]$ in (2), and provide sensitivity signals for the action and critic network training. More details on the mathematical background and training algorithms for ACDs can be found in [23].

For complex power systems, all the states are most likely unavailable even with WAMS. As a result, the system states must be estimated. An autoregressive moving average (ARMA) model (a static function) can then be used to estimate the plant states implicitly and predict the plant outputs at the next step [24], as in

$$\begin{aligned} &\hat{x}(k-m) \sim y(k),...,y(k-m),u(k-1),...,u(k-m) \\ \Rightarrow\ &\hat{x}(k+1) \sim u(k),...,u(k-m),\hat{x}(k-m) \\ &\qquad \sim u(k),...,u(k-m),y(k),...,y(k-m) \\ \Rightarrow\ &\hat{y}(k+1) = N_{FF}[y(k),...,y(k-m),u(k),...,u(k-m)] \end{aligned} \tag{3}$$

where ~ denotes "a function of", m denotes the number of observations needed for state estimation, and N_{FF} denotes the ARMA model implemented from static feed-forward neural networks (FFNNs). As a result, when the three ACD networks are implemented by FFNNs [14], [25], time delayed loops (TDLs) are necessary to provide time delayed inputs, which allows implicit plant state estimation.

B. *Using Recurrent Neural Networks for ACD*

An alternative solution to the ARMA plant state estimation is to directly use a dynamic model without TDLs, such as a recurrent neural network (RNN) as shown in Fig. 2. RNNs have advantages over other static FFNNs in modeling and control of dynamic systems due to their internal dynamic memories [26], [27]. With RNNs, the internal feedback loops effectively provide the time delayed input information for state estimation, as in

$$\begin{aligned} o(k) &= W_o \cdot s(k) \\ &= W_o \cdot f[W_s \cdot s(k-1) + W_i \cdot i(k)], \\ &= N_R[i(k), i(k-1),...] \end{aligned} \tag{4}$$

where $i(k)$ denotes the input vector to the RNN, $o(k)$ denotes the RNN output vector, $s(k)$ denotes the RNN internal state vector, and N_R denotes the equivalent static nonlinear mapping from the RNN's present and historic inputs to its present output.

Fig. 3 shows the RNN-based schematic diagram of a DHP system, where the critic network directly estimates the gradient of $J(k)$ with respect to the plant outputs. For the RNN model network, $o(k)$ in (4) is replaced by $\hat{y}(k+1)$ to achieve one-step-ahead prediction, as in

$$\hat{y}(k+1) = N_{R\_\text{model}}[y(k), y(k-1),...,u(k),u(k-1),...,] \tag{5}$$

where N_{R_model} is the equivalent static mapping N_R produced by the model network, and a similar notation applies to N_{R_action} for the action network and N_{R_critic} for the critic network. From (3),

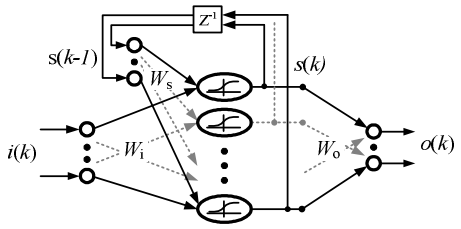

Fig. 2. Structure of a hidden-layer-feedback RNN with no bias terms.

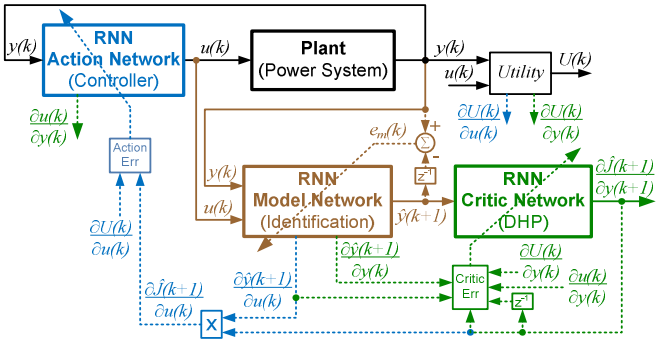

Fig. 3. Schematic diagram of DHP neurocontrol design with RNNs. Color codes: Brown denotes signals for model training, green denotes signals for critic training, and blue denotes signals for action training.

$\hat{y}(k+1)$ in (5) is a function of $\hat{x}(k+1)$ and thus a function of $\hat{x}(k)$ and $u(k)$. Hence, (5) has the necessary mathematical form to reproduce (2).

For the RNN action network shown in Fig. 3,

$$u(k) = N_{R\_\text{action}}[y(k), y(k-1),...]. \tag{6}$$

From the self recursion of (6), i.e.,

$$\begin{aligned} u(k-1) &\sim y(k-2), y(k-3),... \\ u(k-2) &\sim y(k-3), y(k-4),... \end{aligned} \tag{7}$$

the action network thus implements the mapping from [$y(k)$, $y(k$-1),…, $u(k$-1), $u(k$-2),…] to $u(k)$. Hence, from (3), the action network in Fig. 3 has the necessary mathematical form to implement the optimal mapping (optimal control laws) from $\hat{x}(k)$ to u(k).

For the RNN critic network shown in Fig. 3,

$$\hat{\lambda}(k+1) = \frac{\partial \hat{J}(k+1)}{\partial y(k+1)} = N_{R\_\text{critic}}[\hat{y}(k+1), \hat{y}(k),...]. \tag{8}$$

Since $J(k$+1) is a function of $x(k$+1), it is thus a function of [$y(k)$, $y(k$-1),…, $u(k)$, $u(k$-1),…]. With a controller of (6), $J(k$+1) is then a function of [$y(k)$, $y(k$-1),…], and its derivative $\lambda(k$+1) also becomes a function of the same series. Hence, the critic network in Fig. 3, represented by (8), has the necessary mathematical form to approximate $\lambda(k)$.

IV. RNN-DHP Based DOPFC for a 12 Bus Power System

A. *12 Bus Test Power System*

The 12 bus test power system [28] in Fig. 4 is used to

demonstrate the design of a DHP-based DOPFC. No infinite bus is used to hold the system frequency. All four generators are modeled with full dynamics and equipped with automatic voltage regulators (AVRs) and speed governors. Generators 2 to 4 are within the same control area and they are controlled by AGC2. Generator 1 is assumed to be an aggregated representation of an interconnected area and it is controlled by AGC1. With AGC1 and AGC2, the inter-area tie line power flow, P_{tie}, can be maintained at the scheduled value. Block diagrams of the AGC, AVR and speed governor are shown in Fig. 5. All four generators are assumed to be gas turbine based and have a ramp rate (both up and down) of 18 MW/min.

All loads are represented as constant impedance loads, and all lines are represented using the lumped π equivalent model [7]. No system-wide secondary voltage control is implemented, as reactive supports are mostly provided from locally controlled devices scheduled from static optimization such as OPF [7]. The generator and line parameters are provided in [28]. The base case of this system, including the scheduled tie line flow, is defined in the appendix. The system is simulated in the PSCAD/EMTDC environment.

A DHP-based DOPFC is designed below to provide coordinated secondary active and reactive power flow control. Similar to AGC and the secondary voltage control system in Italy, the data update rate for the DOPFC is assumed to be 1 s, which neglects the transient oscillations but includes local controller and load dynamics. AGC2 is disconnected during the training and testing of the DOPFC.

B. Model Network – System Identification

The nonlinear dynamic plant is shown in Fig. 6. The following 11 smoothed wide-area measurements are sampled at 1 Hz for the DOPFC: the system frequency in Hz, f (average rotor speeds of G2, G3 and G4); the 5 load bus voltages in per unit (pu), V_2, V_3, V_4, V_5 and V_6; the tie line power flow in MW, P_{tie}; the active power outputs from G2 to G4 in MW, P_{G2}, P_{G3}, and P_{G4}; and the total line active power losses in MW, P_{loss}. These 11 measurements are then subtracted from a vector consisting of the nominal frequency, voltages and tie line flow, i.e., $y^* = [60, 1, 1, 1, 1, 1, P_{tie}^*, 0, 0, 0, 0]$. After applying a scaling matrix, the plant outputs, $y(k)$, are obtained.

The plant has 6 inputs from the DOPFC. $u_1(k)$ to $u_3(k)$ are adjustment signals to the three generator active power outputs, and $u_4(k)$ to $u_6(k)$ are adjustment signals to the three generator terminal voltages. These inputs are then scaled and added to the steady-state schedules, u^*, from the traditional OPF.

Based on the DHP scheme shown in Fig. 3, an RNN model network, with 17 inputs and 11 outputs, is trained to minimize the following error [23]

$$E_m(k) = \|e_m(k)\|^2 = \|y(k) - \hat{y}(k)\|^2 \quad (9)$$

where $\hat{y}(k)$ is obtained from one step delay of the model network output. The model network is pretrained with pseudo-random binary signal (PRBS) injections at 8 different operating points (OPs), as listed in Table I. Due to the relatively slow responses of generator output power, the PRBS injected to each plant input changes every 60 s with a

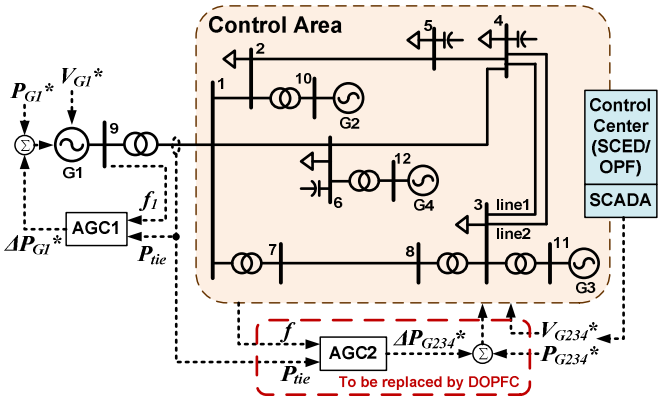

Fig. 4. 12 bus test power system with AGCs.

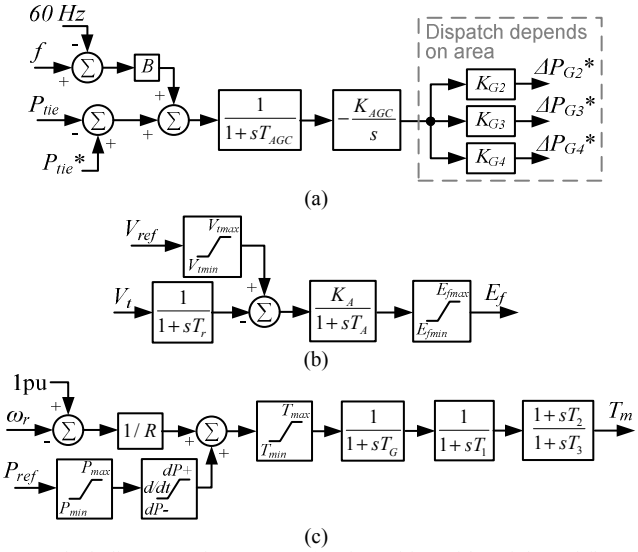

Fig. 5. Block diagrams of a) an AGC (P_{tie} is positive with an inbound flow), b) an AVR, and c) a speed governor.

magnitude between ± 5% of the steady-state schedules. The PRBSs injected to the 6 inputs change sequentially, and as a result, the plant experiences a PRBS perturbation every 10 s. 500 s of data for each operating point are recorded and used for pretraining.

The testing results (with fixed weights) of the pretrained model network at the 8 different operating points are shown in Fig. 7, where only the first output related to the system frequency is plotted due to limited space. The other 10 outputs from the model network have similar tracking performances. After this pretraining stage, the model network is then used to provide sensitivity signals for training the critic and action networks, where the model weights are continuously updated with a small learning rate to ensure tracking of new operating conditions.

C. Cost-to-Go and Critic Network – Control Objective

The control objective for the 12 bus system in this paper includes four components: the total fuel cost, system regulation performances, total line losses, and control effort. The utility function is defined as

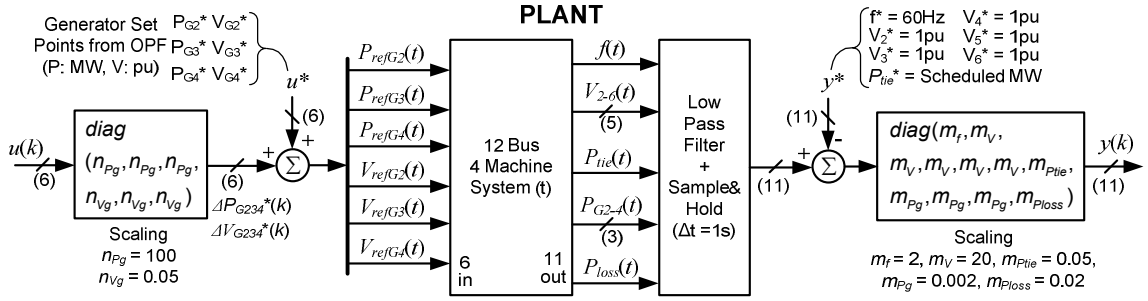

Fig. 6. The nonlinear plant seen by the DHP-based DOPFC in the 12 bus power system example.

TABLE I. OPERATING CONDITIONS FOR MODEL NETWORK PRETRAINING

Oper. Pt.	G2 P_{G2}* (MW)	G2 V_{G2}* (pu)	G3 P_{G3}* (MW)	G3 V_{G3}* (pu)	G4 P_{G4}* (MW)	G4 V_{G4}* (pu)	Load or line changes from base case (P: MW, Q: MVAr)
OP1	500	1.02	200	1.01	300	1.02	None (Base Case)
OP2	400	1.00	250	1.02	350	1.00	None
OP3	550	0.98	175	1.00	275	1.00	None
OP4	500	1.04	250	1.04	350	1.04	P_{L3} = 370, Q_{L3} = 270 P_{L5} = 150, Q_{L5} = 90
OP5	525	1.02	225	1.01	300	1.02	P_{L4} = 370, Q_{L4} = 270
OP6	450	1.00	200	1.00	250	0.98	P_{L2} = 230, Q_{L2} = 170 P_{L6} = 390, Q_{L6} = 270
OP7	500	1.02	200	1.02	300	1.02	One of lines 3-4 is out
OP8	500	1.02	200	1.02	300	1.02	Line 6-4 is out

P_{G1}*, V_{G1}*, and P_{tie}* are unchanged and the same as the base case.

$$U(k) = U_F(k) + U_R(k) + U_L(k) + U_C(k) \tag{10}$$

with

$$\begin{aligned} U_F(k) &= w_{fuel}[F_{G2}(k) + F_{G3}(k) + F_{G4}(k)] \\ U_R(k) &= w_{freq}\Delta f^2(k) + w_{tie}\Delta P_{tie}{}^2(k) + w_{volt} \| \Delta V_{2\text{-}6}(k) \|^2 \\ &= w_{freq} y_1^2(k)/m_f^2 + w_{tie} y_7^2(k)/m_{Ptie}^2 \\ &\quad + w_{volt} \| y_{2\text{-}6}(k) \|^2 / m_V^2 \\ U_L(k) &= w_{loss} P_{loss}(k) = w_{loss} y_{11}(k)/m_{Ploss} \\ U_C(k) &= w_{Pg} \| \Delta P_{G2\text{-}4}{}^*(k) \|^2 + w_{Vg} \| \Delta V_{G2\text{-}4}{}^*(k) \|^2 \\ &= w_{Pg} n_{Pg}^2 \| u_{1\text{-}3}(k) \|^2 + w_{Vg} n_{Vg}^2 \| u_{4\text{-}6}(k) \|^2 \end{aligned} \tag{11}$$

where F_{Gi}(k) is the fuel cost of generator i in \$/MWh, w_x's are various weighting factors (listed in appendix), and m_x's and n_x's are the plant input-output scaling factors as shown in Fig. 6. A quadratic function is used to approximate the generator fuel cost, as in

$$\begin{aligned} F_{Gi}(k) &= a_i + b_i P_{Gi}(k) + c_i P_{Gi}^2(k) \\ &= a_i + b_i y_{6+i}(k)/m_{Pg} + c_i y_{6+i}^2(k)/m_{Pg}^2 \\ &\quad i = 2,3,4 \end{aligned} \tag{12}$$

where the coefficients a_i, b_i and c_i for the three generators are listed in the appendix. From (10) to (12), the utility function depends only on the plant outputs, $y(k)$, and the control actions, $u(k)$. As defined in (1), the cost-to-go function, $J(k)$, is then the discounted accumulation of $U(k)$.

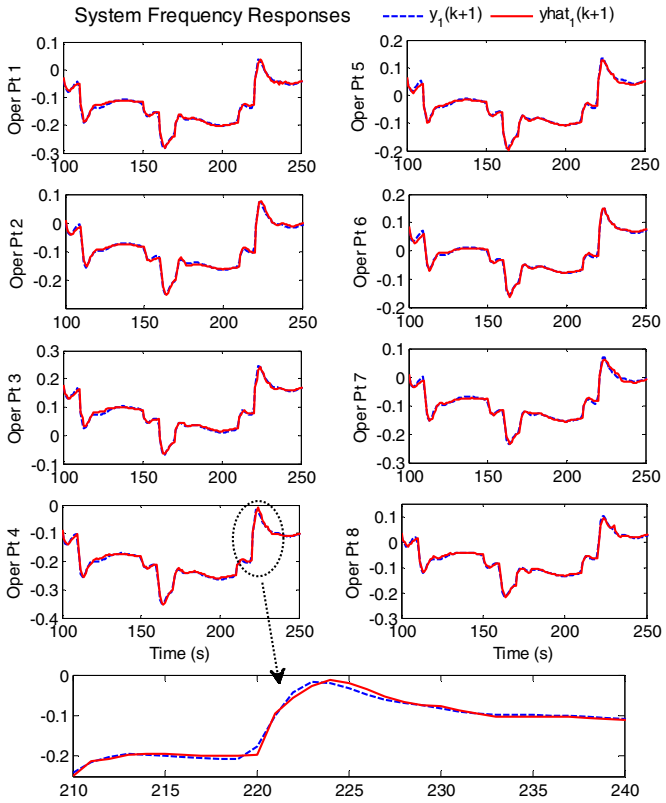

Fig. 7. Model network testing results at the 8 different operating points: system frequency response $y_1(k+1)$ and model network output $yhat_1(k+1)$.

An RNN DHP critic network is trained online to approximate $\lambda(k+1)$, the partial derivative of $J(k+1)$ with respect to $y(k+1)$, by minimizing the following error [23]

$$\begin{aligned} E_c(k) &= \| e_c(k) \|^2 \\ e_c(k) &= \hat{\lambda}(k) - \{ \frac{\partial U(k)}{\partial y(k)} + \frac{\partial U(k)}{\partial u(k)} \frac{\partial u(k)}{\partial y(k)} \\ &\quad + \gamma \hat{\lambda}(k+1) [\frac{\partial \hat{y}(k+1)}{\partial y(k)} + \frac{\partial \hat{y}(k+1)}{\partial u(k)} \frac{\partial u(k)}{\partial y(k)}] \} \end{aligned} \tag{13}$$

The training of the critic network is done online with the action network in loop. The training starts with a small discount factor γ, say 0.5. As the critic weights converge, the discount factor is gradually increased. Since the training of the action network depends on the critic network, these two networks are trained and converge together [25].

D. Action Network – Optimal Control Law Approximation

An RNN action network is trained to approximate the optimal control law by minimizing [23]

$$E_a(k) = \left\| \frac{\partial \hat{J}(k)}{\partial u(k)} \right\|^2 \tag{14}$$

$$\frac{\partial \hat{J}(k)}{\partial u(k)} = \frac{\partial U(k)}{\partial u(k)} + \gamma \hat{\lambda}(k+1) \frac{\partial \hat{y}(k+1)}{\partial u(k)}$$

To minimize the initial impact on the power system, the random initial weights of the critic and action networks are limited to very small values such that the initial outputs of both networks are close to zero. Starting at OP1 (Table I) and a discount factor of 0.5, the action and critic networks are connected to the 12 bus system. Fig. 8 shows the starting process of the two networks. The outputs of both networks (top two graphs of Fig. 8) are initially close to zero with training disabled. At 100 s, the training algorithms for both networks are enabled. As the critic network starts learning the cost-to-go function, its outputs become nonzero, which then makes the action network errors nonzero and starts the action network training process. Different disturbances are then applied to the system. After both networks converge in this operating condition, the training process continues at other operating points and the discount factor is slowly increased.

V. Control Results and Case Studies

A. DOPFC Steady-State Performance at OP1

The steady-state performance of DOPFC is studied at OP1 (see Table I for set points from the control center at OP1). The same optimization objective as $U(k)$ defined in (10) is formulated and solved by the traditional interior-point OPF algorithm in MATPOWER [29]. The voltage and frequency characteristics of the loads are considered in the OPF formulation with the local controller steady-state errors included. The frequency and tie line flow though are fixed at 60 Hz and 480 MW in the OPF solver. This OPF solution gives a benchmark optimal steady-state operating point.

At OP1, the 12 bus system's steady states driven by either AGC2 or DOPFC are compared in Table II with the traditional OPF solution. Note that all three generators have steady-state control errors due to internal losses. With AGC2, although the frequency and P_{tie} are maintained at the nominal/schduled values, the reactive power flow is not controlled, resulting in a relatively low voltage (bolded in Table II) at bus 4. In contrast, the DOPFC is able to control both the steady-state active and reactive power flow much closer to the OPF solution. Note that slightly higher fuel costs are observed in the DOPFC and OPF cases, which is due to the fact that the load bus voltages are raised to closer to unity and thus more energy is consumed.

B. DOPFC Dynamic Performance after Bus 5 Load Tripping

An unexpected contingency happens and causes the 100 MW load at bus 5 to trip at 300 s. To prevent over-voltage, the capacitor bank at bus 5 is tripped at 301 s. The traditional OPF is not able to handle this dynamic event. System frequency and tie line flow control performances by AGC and DOPFC

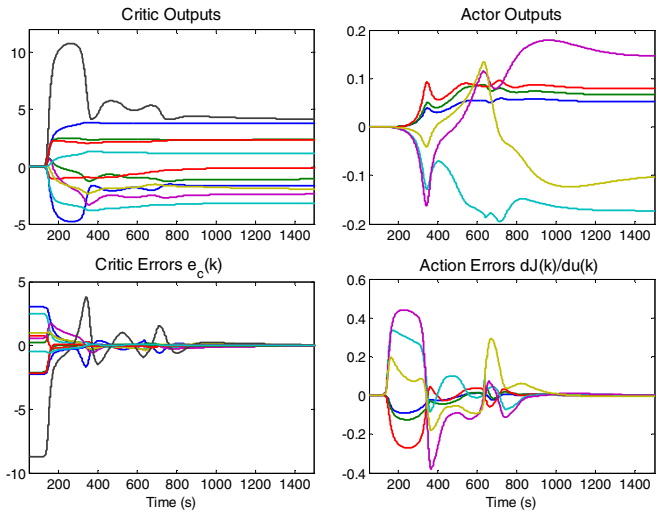

Fig. 8. Starting process of randomly initialized critic and action networks at OP1 with a discount factor of 0.5 (Each curve in the above four graphs represents one scalar in the output/error vector).

TABLE II. Comparison of DOPFC Steady-State Results and Traditional OPF Solutions at OP1

	AGC2	DOPFC	OPF		AGC2	DOPFC	OPF
Utility	3.50	3.22	3.03	P_{tie} (MW)	480.0	480.9	480.0
Fuel (k$/h)	41.35	42.67	42.50	P_{loss} (MW)	45.2	45.1	45.1
f (Hz)	60.00	60.00	60.00	P_{G2} (MW)	492.8	493.3	496.1
V_2 (pu)	0.997	0.996	0.999	P_{G3} (MW)	196.8	211.6	209.8
V_3 (pu)	0.991	1.003	1.005	P_{G4} (MW)	297.0	312.2	307.1
V_4 (pu)	**0.969**	0.981	0.982	V_{G2} (pu)	1.014	1.012	1.015
V_5 (pu)	0.994	1.001	1.001	V_{G3} (pu)	1.010	1.022	1.025
V_6 (pu)	0.988	1.007	0.996	V_{G4} (pu)	1.016	1.037	1.025

are shown in Fig. 9 (a). DOPFC results in a slightly faster frequency recovery.

Fig. 9 (b) shows the G4 output power and terminal voltage during this event. To regulate the short-term power imbalance, AGC decreases G4's generation at its maximum ramp rate. On the other hand, the DHP-based DOPFC further utilizes the load voltage characteristics and intelligently increases G4's terminal voltage, which creates a higher energy consumption at the local bus and balances the short-term over-generation.

C. DOPFC Dynamic Performance with Large Varying Loads at Buses 4&5

In this case, 50 MW and 15 MVAr of load variations, as shown in Fig. 10 (a), are added to buses 4 and 5 between 300 s and 900 s, which are used to simulate the variability contribution from intermittent renewables. As a result, the system experiences large load ramping (both up and down) at a rate of 40 MW/min during this 10 min interval.

With regular AGC, generation from the three generators [Fig. 10 (g)-(i)] vary up and down to follow the system loads without active control on their terminal voltages. Note that the generator terminal voltages also change slightly due to local controller errors [Fig. 10 (j)-(l)]. The frequency and tie line flow are maintained around the nominal values [Fig. 10 (d), (e)], but the voltage at bus 5 [Fig. 10 (c)] varies outside the acceptable range of 0.95-1.05 pu. In this case, if the capacitor

bank at bus 5 is used to regulate the voltage, frequent switching is needed to handle these continuous large variations, which would then greatly shorten the lifetime of the switch devices.

On the other hand, with DOPFC, the generator terminal voltages are also controlled to dynamically track the system's optimal operating point. A lower utility value, as defined in (10), is achieved [Fig. 10 (b)]. The bus 5 voltage is now kept within the acceptable range without degradation on the performances of frequency and tie line power regulations. However, a small operating point drift is observed after this varying load event, as the frequency settles back at 60.01 Hz. In a real power system, as loads and intermittent renewable generations never stop varying, the system frequency will not settle down to a constant value.

VI. Conclusions

An ACD-based DOPFC concept is presented in this paper as a solution to the smart grid operation in a high short-term uncertainty and variability environment. The DOPFC adapts the nonlinear optimal control technique from the ACD theory and provides closed-loop dynamic tracking of a power system's optimal operating point. Characteristics and dynamics of local controller and load are inherently incorporated with the continuous online learning of the ACD method. A dual heuristic programming ACD approach using recurrent neural networks is used to design the DOPFC for a 12 bus test power system. Simulation results demonstrate the promising steady-state and dynamic performances of the designed DOPFC as compared to the traditional OPF and AGC.

Appendix

Base case and generator fuel cost coefficients of the 12 bus power system (modified from [27]):

Bus	V_G* (pu)	P_G* (MW)	Fuel Cost ($/h) a	b	c	Load (MVA)	Shunt (MVAr)
2						280 + j200	
3						320 + j240	
4						320 + j240	160
5						100 + j60	80
6						440 + j300	180
9 (G1)	1.02	480					
10 (G2)	1.02	500	700	34.10	0.0117		
11 (G3)	1.01	200	670	36.85	0.0135		
12 (G4)	1.02	300	650	36.24	0.0130		

Scheduled area power import P_{tie}* = 480 MW.

Weighting factors used in the utility function:

w_{fuel}	w_{freq}	w_{tie}	w_{volt}	w_{loss}	w_{Pg}	w_{Vg}
5e-5	80	0.025	800	0.01	1e-4	200

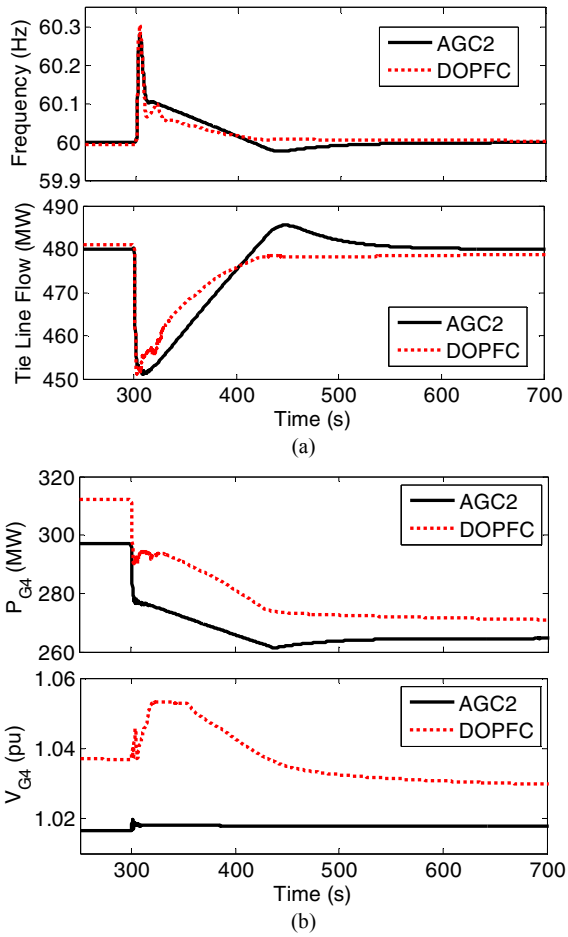

Fig. 9. System performances after bus 5 load tripping: (a) frequency and tie line power flow, (b) G4 output powers and its terminal voltages.

References

[1] D. Maggio, C. D'Annunzio, S. Huang, C. Thompson, "Outstanding questions around increasing variable generation penetration in the ERCOT system," in *Proc. 2010 IEEE PES General Meeting*, Minneapolis, MN, 25-29 Jul. 2010.

[2] D. Hawkins, K. Parks, and J. Blatchford, "Improved power system operations with high penetration of wind power: a dialog between academia and industry," in *Proc. 2010 IEEE PES General Meeting*, Minneapolis, MN, 25-29 Jul. 2010.

[3] K. Porter and J. Rogers, "Status of centralized wind power forecasting in North America: May 2009 - May 2010," NREL subcontract report, NREL/SR-550-47853, Apr 2010.

[4] S. Fink, C. Mudd, K. Porter, and B. Morgenstern, "Wind energy curtailment case studies," NREL subcontract report, NREL/SR-550-46716, Oct. 2009.

[5] J. Momoh, M. El-Hawary, and R. Adapa, "A review of selected optimal power flow literature to 1993. I. Nonlinear and quadratic programming approaches," *IEEE Trans. Power Syst.*, vol. 14, no. 1, pp. 96-104, Feb. 1999.

[6] J. Momoh, R. Adapa, and M. El-Hawary, "A review of selected optimal power flow literature to 1993. II. Newton, linear programming and interior point methods," *IEEE Trans. Power Syst.*, vol. 14, no. 1, pp. 105-111, Feb. 1999.

[7] P. Kundur, "Power system stability and control," New York: McGraw-Hill, 1994. ISBN-13: 978-0070359581.

[8] J. De La Ree, V. Centeno, J. Thorp, and A. Phadke, "Synchronized phasor measurement applications in power systems," *IEEE Trans. Smart Grid*, vol. 1, no. 1, pp. 20-27, Jun. 2010.

[9] X. Xie, Y. Xin, J. Xiao, J. Wu, and Y. Han, "WAMS applications in Chinese power systems," *IEEE Power Energy Mag.*, vol. 4, no. 1, pp. 54-63, Jan.-Feb. 2006.

[10] K. Tomsovic, D. Bakken, V. Venkatasubramanian, and A. Bose, "Designing the next generation of real-time control, communication, and computations for large power systems," *Proc. IEEE*, vol. 93, no. 5, pp. 965-979, May 2005.

[11] I. Kamwa, R. Grondin, and Y. Hébert, "Wide-Area measurement based

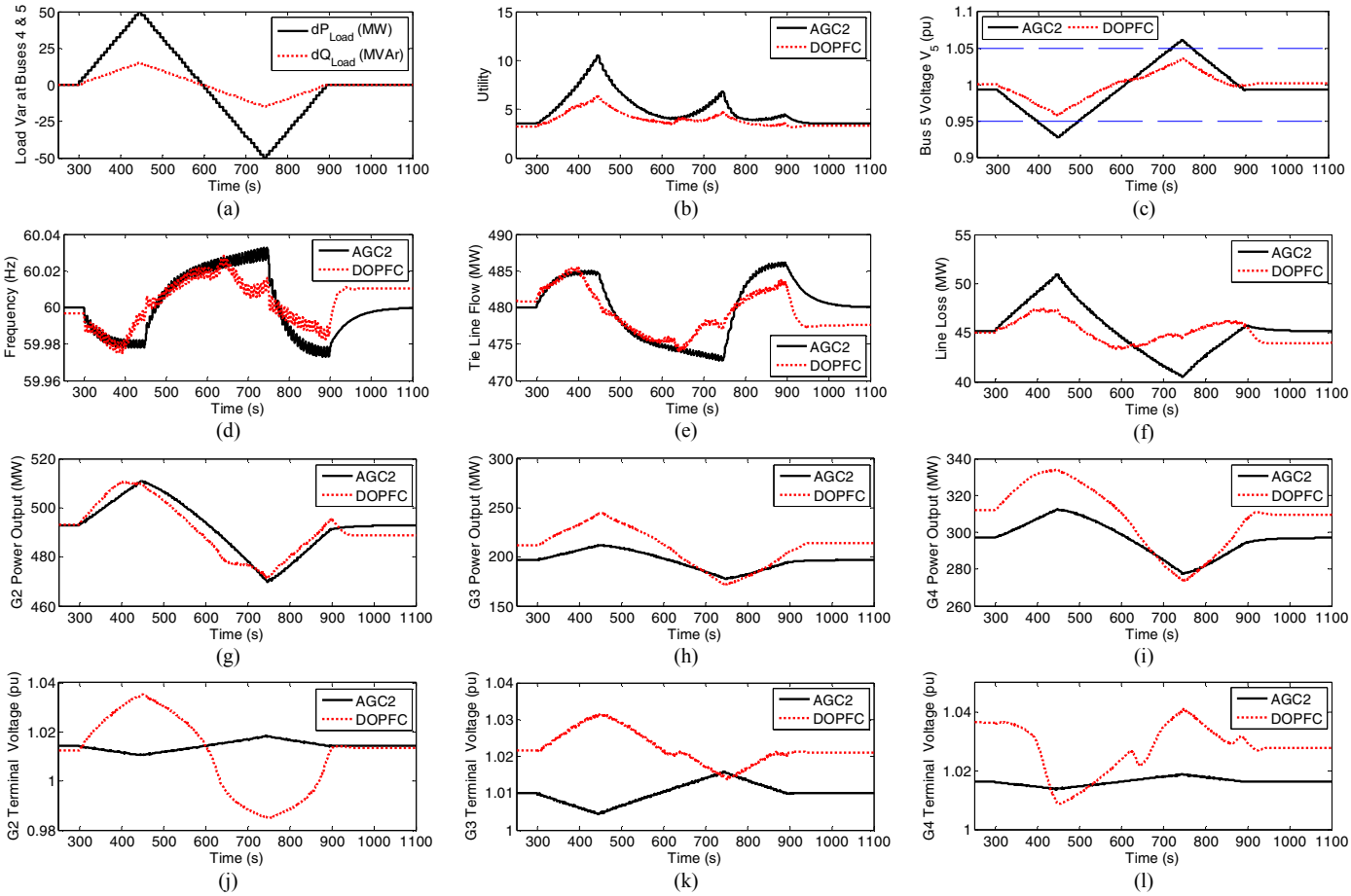

Fig. 10. The 12 bus power system performances during large load variations at buses 4 and 5.

stabilizing control of large power systems - a decentralized/hierarchical approach," *IEEE Trans. Power Syst.*, vol. 16, no. 1, pp. 136–153, Feb. 2001.

[12] H. Ni, G. Heydt, and L. Mili, "Power system stability agents using robust wide area control," *IEEE Trans. Power Syst.*, vol. 17, no. 4, pp. 1123–1131, Nov. 2002.

[13] B. Chaudhuri, R. Majumder, and B. C. Pal, "Wide-Area measurement based stabilizing control of power system considering signal transmission delay," *IEEE Trans. Power Syst.*, vol. 19, no. 4, pp. 1971–1979, Nov. 2004.

[14] S. Mohagheghi, G. Venayagamoorthy, and R. Harley, "Optimal Wide Area Controller and State Predictor for a Power System," *IEEE Trans. Power Syst.*, vol. 22, no. 2, pp. 693-705, May 2007.

[15] S. Corsi, M. Pozzi, C. Sabelli, and A. Serrani, "The coordinated automatic voltage control of the Italian transmission grid-part I: reasons of the choice and overview of the consolidated hierarchical system," *IEEE Trans. Power Syst.*, vol. 19, no. 4, pp. 1723-1732, Nov. 2004.

[16] S. Corsi, M. Pozzi, M. Sforna, and G. Dell'Olio, "The coordinated automatic voltage control of the Italian transmission grid-part II: control apparatuses and field performance of the consolidated hierarchical system," *IEEE Trans. Power Syst.*, vol. 19, no. 4, pp. 1733-1741, Nov. 2004.

[17] M. Begovic, D. Novosel, D. Karlsson, C. Henville, and G. Michel, "Wide-area protection and emergency control," *Proc. IEEE*, vol. 93, no. 5, pp. 876-891, May 2005.

[18] B. Fardanesh, "Future trends in power system control," *IEEE Computer Applications in Power*, vol. 15, no. 3, pp. 24-31, Jul. 2002.

[19] D. Prokhorov and D. Wunsch, "Adaptive critic designs," *IEEE Trans. Neural Networks*, vol. 8, no. 5, pp. 997-1007, Sep. 1997.

[20] P. Werbos, "New directions in ACDs: keys to intelligent control and understanding the brain," in *Proc. Int'l Joint Conf. Neural Networks (IJCNN) 2000*, vol. 3, pp. 61-66, Como, Italy, 24 Jul. 2000.

[21] G. K. Venayagamoorthy, "CAREER: Scalable learning and adaptation with intelligent techniques and neural networks for reconfiguration and survivability of complex systems," NSF CAREER Award ECCS # 0348221, Jun. 2004 (submitted to NSF in July 2003).

[22] G. K. Venayagamoorthy, "Dynamic optimization of a multimachine power system with a FACTS device using identification and control ObjectNets", in *Proc. 39th IEEE IAS Annual Meeting on Industry Applications*, Seattle, USA, October 2004, pp. 2643 – 2650.

[23] J. Si, A. Barto, W. Powell, and D. Wunsch, Eds. "Hanbook of learning and approximate dynamic programming", Wiley-IEEE Press, 2004. ISBN-13: 978-0471660545.

[24] K. Narendra, "Neural networks for control theory and practice," *Proc. IEEE*, vol. 84, no. 10, pp. 1385-1406, Oct. 1996.

[25] G. Venayagamoorthy, R. Harley, and D. Wunsch, "Implementation of adaptive critic-based neurocontrollers for turbogenerators in a multimachine power system," *IEEE Trans. Neural Networks*, vol. 14, no. 5, pp. 1047-1064, Sep 2003.

[26] D. Prokhorov, G. Puskorius, and L. Feldkamp, "Dynamical neural networks for control," in *A Field Guide to Dynamical Recurrent Networks*, Wiley-IEEE Press, 2001. ISBN-13: 978-0780353695.

[27] J. Liang, J. Dai, G. Venayagamoorthy, and R. Harley, "Dynamic system eigenvalue extraction using a linear echo state network for small-signal stability analysis – a novel application," in *Proc. IEEE Int'l Joint Conf. Neural Networks (IJCNN) 2010*, Barcelona, Spain, 18-23 Jul. 2010.

[28] S. Jiang, U. Annakkage, and A. Gole, "A platform for validation of FACTS models," *IEEE Trans. Power Delivery*, vol. 21, no. 1, pp. 484-491, Jan 2006.

[29] R. Zimmerman, "MATPOWER user's manual," May 2010, [Online]. Available: http://www.pserc.cornell.edu/matpower/manual.pdf.